



# ATLAS NOTE

## ATLAS-CONF-2011-151

November 12, 2011



### Search for a charged Higgs boson decaying via $H^+ \rightarrow \tau_{\text{lep}} + \nu$ in $t\bar{t}$ events with one or two light leptons in the final state using $1.03 \text{ fb}^{-1}$ of $pp$ collision data recorded at $\sqrt{s} = 7 \text{ TeV}$ with the ATLAS detector

The ATLAS Collaboration

#### Abstract

This paper presents the results of a search for charged Higgs bosons by the ATLAS experiment, based on  $1.03 \text{ fb}^{-1}$  of proton-proton collision data at  $\sqrt{s} = 7 \text{ TeV}$  using the single-lepton and dilepton channels in  $t\bar{t}$  decays with a leptonically decaying  $\tau$  in the final state. The data agree with the Standard Model expectation. Assuming  $\mathcal{B}(H^+ \rightarrow \tau\nu) = 1$ , this leads to upper limits on the branching fraction  $\mathcal{B}(t \rightarrow bH^+)$  between 5.2% and 14.1% for  $H^+$  masses in the range  $90 \text{ GeV} < m_{H^+} < 160 \text{ GeV}$ . In the context of the  $m_h^{\text{max}}$  scenario of the MSSM, values of  $\tan\beta$  larger than 30–56 are excluded for  $H^+$  masses in the range  $90 \text{ GeV} < m_{H^+} < 140 \text{ GeV}$ .

# 1 Introduction

Charged Higgs bosons<sup>1</sup>,  $H^+$  and  $H^-$ , are predicted by several non-minimal Higgs scenarios [1, 2], such as models containing Higgs triplets and Two-Higgs-Doublet Models (2HDM) [3]. The observation of charged Higgs bosons would clearly indicate physics beyond the Standard Model (SM). The analysis presented in this note considers the type-II 2HDM, which is also the Higgs sector of the Minimal Supersymmetric Standard Model (MSSM) [4]. For charged Higgs boson masses smaller than the top-quark mass ( $m_{H^+} < m_{\text{top}}$ ), the dominant production mode at the Large Hadron Collider (LHC) for  $H^+$  is through the top-quark decay  $t \rightarrow bH^+$ . The dominant source of top-quarks at the LHC is through  $t\bar{t}$  production. The cross section for charged Higgs boson production from single top-quark events is much smaller and not considered here. For  $\tan\beta > 3$ , where  $\tan\beta$  is the ratio of the vacuum expectation values of the two Higgs doublets, charged Higgs bosons decay mainly via  $H^+ \rightarrow \tau\nu$  [5]. In this note, we always consider  $\mathcal{B}(H^+ \rightarrow \tau\nu) = 1$ . With this assumption, the combined LEP lower limit for the charged Higgs boson mass is about 90 GeV [6]. At the Tevatron, searches for MSSM Higgs bosons in  $p\bar{p}$  collisions cover regions of the MSSM parameter space with either a small (below 1.5) or large (above 30)  $\tan\beta$ , but no evidence for charged Higgs bosons has been found. Hence, the Tevatron experiments placed upper limits in the 15–20% range on  $\mathcal{B}(t \rightarrow bH^+)$  [7, 8]. In addition, preliminary results of charged Higgs boson searches in top-quark decays have recently been made public by the CMS experiment [9], and also by ATLAS in the  $t\bar{t} \rightarrow b\bar{b}WH^+ \rightarrow b\bar{b}qq'\tau_{\text{had}}\nu$  and  $t\bar{t} \rightarrow b\bar{b}WH^+ \rightarrow b\bar{b}\ell\nu c\bar{s}$  channels [10, 11].

This note describes the search for charged Higgs bosons in  $t\bar{t}$  events with one or two light charged leptons (i.e. electrons or muons, hereafter referred to as  $l$ ) in the final state, using data from proton-proton collisions at  $\sqrt{s} = 7$  TeV, collected in 2011 with the ATLAS experiment [12] at the LHC. If the charged Higgs boson arising from  $t \rightarrow bH^+$  solely decays into  $\tau\nu$ , a small increase in the branching fraction for single-lepton and dilepton decays of  $t\bar{t}$  pairs occurs, as the  $\tau$  decays leptonically more often than the  $W$  boson:  $\mathcal{B}(H^+ \rightarrow \tau\nu \rightarrow l + N\nu) \simeq 35\%$  while  $\mathcal{B}(W \rightarrow l + N\nu) \simeq 25\%$ . However, viable search strategies for charged Higgs bosons do not only rely on the presence or absence of an excess of single-lepton and dilepton  $t\bar{t}$  events, as compared to the SM predictions. It is also useful to identify discriminating variables that allow a distinction between leptons produced in  $\tau \rightarrow l\nu/\nu\tau$  (e.g. in decays of  $W$  or charged Higgs bosons) and leptons arising directly from  $W$  boson decays.

One such discriminating variable is the invariant mass  $m_{bl}$  of a  $b$ -quark and a light charged lepton  $l$  (electron or muon) coming from the same top-quark, or more conveniently  $\cos\theta_l^*$  defined as:

$$\cos\theta_l^* = \frac{2m_{bl}^2}{m_{\text{top}}^2 - m_W^2} - 1 \simeq \frac{4p^b \cdot p^l}{m_{\text{top}}^2 - m_W^2} - 1 \text{ with } p^b \cdot p^l = 2E_b E_l (1 - \cos\theta_{bl}) = 4E_b E_l \sin^2(\theta_{bl}/2), \quad (1)$$

where  $p^b$  and  $p^l$  are the four-momenta of the  $b$ -quark and of the lepton  $l$  (they can be chosen in any reference frame, since  $\cos\theta_l^*$  contains an invariant product) and  $\theta_{bl}$  is the angle between them. Note that both  $m_b^2$  and  $m_l^2$  are neglected, hence  $m_{bl}^2 \simeq 2p^b \cdot p^l$ . This variable is commonly used to measure the polarisation of  $W$  bosons in top-quark decays [13], where  $\theta_l^*$  is the angle of the lepton momentum with respect to the helicity axis in the  $W$  rest frame. In this analysis, we use the same variable  $\cos\theta_l^*$  for other purposes. Indeed, if a top-quark decay is mediated through an  $H^+$  and if the  $H^+$  is heavier than the  $W$  boson, the  $b$ -quark usually has a smaller momentum than in the case of a  $W$ -mediated top-quark decay. Also, a light charged lepton  $l$  arising from a  $\tau$  decay is likely to have a smaller momentum than a lepton coming directly from a real  $W$  boson. As a result, the presence of a charged Higgs boson in a leptonic quark decay strongly reduces the invariant product  $p^b \cdot p^l$ , leading to  $\cos\theta_l^*$  values mostly close to  $-1$ .

---

<sup>1</sup>In the following, charged Higgs bosons will be denoted  $H^+$ , with the charge-conjugate  $H^-$  always implied.

We also introduce two new transverse mass observables that can help discriminate leptons produced in  $H^+ \rightarrow \tau\nu$  decays from leptons coming from  $W$  bosons [14]. These two variables,  $m_T^H$  (for single-lepton events) and  $m_{T2}^H$  (for dilepton events), were measured in ATLAS data for the first time in 2010 [15].

In single-lepton  $t\bar{t}$  events where a  $W$  boson decays directly into an electron or muon and one neutrino, the so-called  $W$  transverse mass is obtained by constraining the (squared) missing mass  $(p^{\text{miss}})^2$  to be zero, assuming that it only comes from the massless neutrino associated with the direct  $W$  decay:

$$(m_T^W)^2 = \min_{\substack{\{p_z^{\text{miss}}, E^{\text{miss}}\} \\ \{(p^{\text{miss}})^2 = 0\}}} [(p^l + p^{\text{miss}})^2] = 2p_T^l E_T^{\text{miss}} (1 - \cos \phi_{l,\text{miss}}). \quad (2)$$

Here  $p_z^{\text{miss}}$  and  $E^{\text{miss}}$  are the longitudinal momentum and the energy of the neutrino,  $p_T^l$  and  $E_T^{\text{miss}}$  are the transverse momenta of the lepton and the neutrino,  $\phi_{l,\text{miss}}$  being the azimuthal angle between them. In the case of a leptonic  $\tau$  decay (either from a  $W$  or charged Higgs boson), this constraint is not valid since the missing momentum comes from three neutrinos, hence  $(p^{\text{miss}})^2 \neq 0$ . However, if one of the two  $b$ -quarks can be associated with the leptonically decaying top-quark, one can compute a so-called *charged Higgs boson transverse mass* by performing a maximisation of the invariant mass  $(p^l + p^{\text{miss}})^2$ , now using the longitudinal momentum and the energy of all neutrinos (again referred to as  $p_z^{\text{miss}}$  and  $E^{\text{miss}}$ ) in the single-lepton  $t\bar{t}$  event:

$$(m_T^H)^2 = \max_{\substack{\{p_z^{\text{miss}}, E^{\text{miss}}\} \\ \{(p^{\text{miss}} + p^l + p^b)^2 = m_{\text{top}}^2\}}} [(p^l + p^{\text{miss}})^2]. \quad (3)$$

The explicit expression of the charged Higgs boson transverse mass is:

$$(m_T^H)^2 = \left( \sqrt{m_{\text{top}}^2 + (\vec{p}_T^l + \vec{p}_T^b + \vec{p}_T^{\text{miss}})^2} - p_T^b \right)^2 - (\vec{p}_T^l + \vec{p}_T^{\text{miss}})^2. \quad (4)$$

In dilepton  $t\bar{t}$  events, the final state includes two leptons and missing energy on both sides of the event, making its full reconstruction more complicated. With one top-quark decaying into  $\bar{b}W$  and the other one into  $bH^+$ , if  $\ell$  stands for  $e, \mu$  or  $\tau$ , we have the following set of six constraints:

$$\begin{aligned} (p^{H^+} + p^b)^2 &= m_{\text{top}}^2, \\ (p^{\ell^-} + p^{\bar{\nu}_\ell})^2 &= m_W^2, \\ (p^{\ell^-} + p^{\bar{\nu}_\ell} + p^b)^2 &= m_{\text{top}}^2, \\ (p^{\bar{\nu}_\ell})^2 &= 0, \\ \vec{p}_T^{H^+} - \vec{p}_T^{\ell^+} + \vec{p}_T^{\bar{\nu}_\ell} &= \vec{p}_T^{\text{miss}}. \end{aligned} \quad (5)$$

Here,  $p^{H^+}$  and  $p^{\bar{\nu}_\ell}$  are the unknown quantities in the event. The system of constraints above leaves two free parameters (compared to only one in the single-lepton case) over which we maximise the charged Higgs boson mass to obtain the *generalised charged Higgs boson transverse mass*. If we choose one of the free parameters to be the  $z$ -component of the charged Higgs boson momentum, we perform the maximisation over it, using the result of the single-lepton case, hence  $m_{T2}^H$  is equivalent to:

$$m_{T2}^H = \max_{\{\text{constraints}\}} [m_T^H(\vec{p}_T^{H^+})], \quad (6)$$

where we have defined:

$$(m_T^H(\vec{p}_T^{H^+}))^2 = \left( \sqrt{m_{\text{top}}^2 + (\vec{p}_T^{H^+} + \vec{p}_T^b)^2} - p_T^b \right)^2 - (\vec{p}_T^{H^+})^2. \quad (7)$$

The maximisation over the remaining parameter is performed numerically, after having assigned each of the two  $b$ -quarks to its corresponding charged lepton.

The transverse masses  $m_T^H$  and  $m_{T2}^H$  are larger than the true charged Higgs boson mass  $m_{H^+}$  and smaller than the top-quark mass used in the constraints,  $m_{\text{top}}$ . Therefore, they can serve as discriminants between top-quark decays mediated by a  $W$  or charged Higgs boson, based on their different masses.

In Section 2, we discuss the Monte Carlo and data samples used in our study. In Section 3, we describe the reconstruction of physics objects in ATLAS and, in Section 4, a data-driven method aimed at deriving backgrounds containing fake leptons is presented. Section 5 deals with the measurement of  $\cos \theta_l^*$  and  $m_T^H$  in ATLAS data and Monte Carlo simulated events, based on a single-lepton  $t\bar{t}$  event topology. In Section 6, we repeat a similar analysis, where  $\cos \theta_l^*$  and  $m_{T2}^H$  are measured in dilepton  $t\bar{t}$  events. Assuming  $\mathcal{B}(H^+ \rightarrow \tau\nu) = 1$ , upper limits on the branching fraction  $\mathcal{B}(t \rightarrow bH^+)$  at the 95% confidence level are presented in Section 7. Finally, a summary is given in Section 8.

## 2 Monte Carlo and Data Samples

The background processes that enter the search for a charged Higgs boson in  $t\bar{t}$  events with one or two leptons include the production of  $t\bar{t} \rightarrow b\bar{b}W^+W^-$ , single top-quark events, the production of  $Z/\gamma^*+\text{jets}$  and  $W+\text{jets}$ , diboson events, as well as QCD multijet events with fake leptons (see Section 4).

The Monte Carlo samples for  $t\bar{t}$  and single top-quark events are generated using the MC@NLO [16] generator. The top-quark mass is set to 172.5 GeV, and the parton density function is CTEQ66 [17]. The parton shower and the underlying event are added using HERWIG [18] and JIMMY [19], respectively. The (inclusive)  $t\bar{t}$  cross section is normalised to the approximate next-to-next-to-leading-order (NNLO) prediction of 165 pb [20, 21]. For the single top-quark production, no K-factors are applied to the cross sections predicted by the MC@NLO generator, which are 66.2 pb, 4.3 pb and 14.6 pb for the inclusive  $t$ -,  $s$ - and  $Wt$ -production channels, respectively. The so-called diagram removal scheme is used in order to account for the overlaps between single top-quark and  $t\bar{t}$  final states [22].

Single vector boson production is simulated using ALPGEN [23] interfaced to HERWIG/JIMMY for the underlying event model. The parton density function CTEQ6.1 [24] is used for matrix element calculations and parton shower evolution. The additional partons produced in the matrix element part of the event generation can be light partons or heavy quarks. The production cross sections of all samples are rescaled by 1.20 and 1.25, respectively, in order to match NNLO calculations. Diboson events ( $WW$ ,  $WZ$  and  $ZZ$ ) are generated and hadronised using HERWIG. For these events, inclusive decays are used for both gauge bosons, and a filter is applied at the generator level, requiring at least one electron or muon with  $p_T > 10$  GeV and a pseudorapidity  $|\eta| < 2.8$ . K-factors (1.48 for  $WW$ , 1.60 for  $WZ$ , 1.30 for  $ZZ$ ) are used to match next-to-leading-order cross section predictions.

The SM background samples used in this study are summarised in Table 1. In addition, three types of signal samples are produced with PYTHIA [25] for  $m_{H^+}$  between 90 and 160 GeV:  $t\bar{t} \rightarrow b\bar{b}H^+W^-$ ,  $t\bar{t} \rightarrow b\bar{b}H^-W^+$  and  $t\bar{t} \rightarrow b\bar{b}H^+H^-$ . The charged Higgs boson decay mode is always  $H^+ \rightarrow \tau\nu$ . When a top-quark decays into  $Wb$ , the  $W$  boson subsequently decays inclusively. In addition, TAUOLA [26] is used for  $\tau$  decays, and PHOTOS [27] is used for photon radiation from charged leptons.

Event generators are tuned to describe ATLAS data: the parameter sets AMBT1 [28] and AUET1 [29] are used for the events hadronised with PYTHIA and HERWIG/JIMMY, respectively.

All Monte Carlo events are propagated through a detailed GEANT4 simulation [30,31] of the ATLAS detector, and they are reconstructed with the same algorithms as the data. Only data taken with all ATLAS subsystems fully operational are used for this analysis. Together with the requirement of having  $pp$  collisions at 7 TeV in stable beam conditions, this results in a data sample of  $1.03 \pm 0.04 \text{ fb}^{-1}$  for the 2011 data-taking period considered here [32]. The LHC peak luminosity exceeded  $10^{32} \text{ cm}^{-2}\text{s}^{-1}$  over the whole data-taking period, a level at which more than one interaction per bunch crossing occurs (on average, between 5 and 6 during the data-taking period considered here). In addition, the LHC ran with an in-train bunch separation of 50 ns. Hence, the out-of-time pile-up (i.e. overlapping signals in the detector from other neighboring bunch crossings) is also important. In order to take into account the pile-up, minimum bias events are added to the hard process in each Monte Carlo sample. Prior to the analysis, the simulated events are reweighted to a given data sample, using the average number of pile-up interactions.

Process	Generator	Cross section (in pb)
$t\bar{t}$ with at least one lepton $\ell = e, \mu, \tau$	MC@NLO	89.7
Single top-quark $Wt$ -channel (inclusive)	MC@NLO	14.6
Single top-quark $t$ -channel (with $\ell$ )	MC@NLO	21.3
Single top-quark $s$ -channel (with $\ell$ )	MC@NLO	1.4
$W \rightarrow \ell\nu + \text{jets}$	ALPGEN	$3.1 \times 10^4$
$Z/\gamma^* \rightarrow \ell\ell + \text{jets}, m(\ell\ell) > 10 \text{ GeV}$	ALPGEN	$1.5 \times 10^4$
$WW$	HERWIG	17.0
$ZZ$	HERWIG	1.3
$WZ$	HERWIG	5.5

Table 1: Cross sections for the SM background Monte Carlo samples.

### 3 Object Reconstruction in ATLAS

The ATLAS detector consists of an inner tracking detector with an acceptance  $|\eta| < 2.5$  surrounded by a thin 2 T superconducting solenoid, a calorimeter system extending up to  $|\eta| = 4.9$  that uses a variety of technologies to detect electrons, photons and hadronic jets, as well as a large muon spectrometer using superconducting toroids arranged with an eight-fold azimuthal coil symmetry.

#### 3.1 Trigger

The analysis presented here relies on events passing a single-lepton (electron or muon) trigger, with a  $p_T$  threshold at 20 GeV for the electron trigger and at 18 GeV for the muon trigger. These thresholds are low enough to guarantee that electrons with  $E_T > 25 \text{ GeV}$  and muons with  $p_T > 20 \text{ GeV}$  are in the plateau region of the trigger-efficiency curve.

#### 3.2 Data quality

Following the basic data quality checks, further event cleaning is performed by demanding that no jet be consistent with having originated from instrumental effects, such as spikes in the hadronic end-cap calorimeter, coherent noise in the electromagnetic calorimeter, or non-collision backgrounds. In order to further reject the non-collision backgrounds, only events with a reconstructed primary vertex with at least five associated tracks are considered.

### 3.3 Electrons

Electrons are reconstructed by matching clustered energy deposits in the electromagnetic calorimeter to tracks reconstructed in the inner detector. They are required to meet quality requirements based on the expected shower shape of electrons [33]. Electrons are required to have  $E_T > 15$  GeV, and be isolated (by requiring less than 3.5 GeV of transverse energy – after corrections for pile-up and leakage – in a cone of  $\Delta R = 0.2$  around the electron<sup>2</sup>, excluding the energy deposit from the electron itself). Electrons are required to be in the fiducial volume of the detector,  $|\eta| < 2.47$  (the transition region between the barrel and end-cap calorimeters,  $1.37 < |\eta| < 1.52$ , is excluded).

### 3.4 Muons

Muon candidates are required to have a match of an inner detector track with a track reconstructed in the muon spectrometer [34]. Candidates are required to have  $p_T > 15$  GeV and  $|\eta| < 2.5$ . Only isolated muons are accepted by requiring that, in a cone of  $\Delta R = 0.3$  around the muon (excluding the energy deposit from the muon itself), both the transverse energy deposited in the calorimeters and the transverse momentum of all inner detector tracks amount to less than 4 GeV. Finally, muon candidates are rejected if they are found within  $\Delta R < 0.4$  of any jet with  $p_T > 20$  GeV.

### 3.5 Jets

Jets are reconstructed with the anti- $k_t$  algorithm [35, 36] with a size parameter value of  $R = 0.4$ . The jet finder uses three-dimensional noise-suppressed clusters [37] in the calorimeter, reconstructed at the electromagnetic energy scale. The jets are then calibrated to the hadronic energy scale with correction factors based on Monte Carlo simulations [38], which depend on their transverse momentum ( $p_T$ ) and their pseudorapidity ( $\eta$ ). Jets with an axis within  $\Delta R < 0.2$  of the direction of an electron are rejected in order to avoid overlap between electrons and jets.

In order to identify the jets initiated by  $b$ -quarks, a high-performance tagger [39] combining impact-parameter information with the explicit determination of an inclusive secondary vertex, is used. The cut point is determined to give a nominal efficiency of about 70% for  $b$ -jets with  $p_T > 20$  GeV in  $t\bar{t}$  events. Since the  $b$ -tagger relies on the inner tracking detectors, the pseudorapidity acceptance region must be restricted to  $|\eta| < 2.5$ .

### 3.6 Missing transverse energy

The missing transverse energy  $E_T^{\text{miss}}$  [40] is reconstructed from three-dimensional noise-suppressed clusters in the calorimeter, calibrated at the electromagnetic energy scale, and from muons reconstructed in the muon spectrometer. In the  $E_T^{\text{miss}}$  calculation, calorimeter clusters belonging to jets with  $p_T > 20$  GeV are then calibrated to the hadronic energy scale. Calorimeter cells not associated with any object are also taken into account and calibrated at the electromagnetic energy scale. Muons reconstructed from the inner tracking detectors are used to recover muons in regions not covered by the spectrometer and, in order to deal appropriately with the energy deposited by muons in the calorimeters, the muon term of  $E_T^{\text{miss}}$  is calculated differently for isolated and non-isolated muons.

---

<sup>2</sup> $\Delta R = \sqrt{(\Delta\eta)^2 + (\Delta\phi)^2}$ , where  $\Delta\eta$  is the difference in pseudorapidity of the two objects in question, and  $\Delta\phi$  the difference of their azimuthal angles.

## 4 Data-Driven Estimation of Backgrounds with Mis-Identified Leptons

In order to give a realistic picture of the impact of the backgrounds with mis-identified leptons, methods using the actual data recorded by the detector are applied, e.g. because lepton isolation variables are difficult to simulate. The excellent lepton identification by ATLAS is exploited in this analysis, as the trigger and the event selection are both based on the identification of at least one isolated lepton. However, there is also a non-negligible contribution from non-isolated leptons, arising from the semileptonic decay of a  $b$  or  $c$  hadron, from the decay-in-flight of a  $\pi^\pm$  or  $K$ -meson and, in the case of fake electron objects, from the reconstruction of a  $\pi^0$ , photon conversion and shower fluctuations. All leptons coming from such mechanisms are referred to as *fake* leptons, as opposed to true isolated leptons (e.g. from the decay of  $W$  and  $Z$  bosons) which are referred to as *real* leptons. The fundamental idea of the data-driven method discussed here is to use differences in the properties related to the lepton identification between real and fake electrons or muons. For this purpose, two data samples are defined, differing only in the lepton identification criteria. The first sample contains mostly events with real leptons and is referred to as the *tight* sample. The second one contains mostly events with fake leptons and is referred to as the *loose* sample. In this analysis, the loose sample is simply obtained by loosening the isolation requirement for the leptons.

In the single-lepton channel, QCD multijet events, in which a jet is mis-identified as a lepton, may constitute a non-negligible background. Let  $N_r^L$  and  $N_f^L$  (respectively  $N_r^T$  and  $N_f^T$ ) be the numbers of events containing real and fake leptons passing a loose (respectively tight) selection. The number of events containing one loose or tight lepton can be written as:

$$N^L = N_f^L + N_r^L, \quad (8)$$

$$N^T = N_f^T + N_r^T. \quad (9)$$

Let  $r$  and  $f$  be the rates for a real or fake lepton to be identified as a tight lepton:

$$r = \frac{N_r^T}{N_r^L} \quad \text{and} \quad f = \frac{N_f^T}{N_f^L}. \quad (10)$$

The number of fake leptons passing the tight selection  $N_f^T$  can then be re-written as:

$$N_f^T = \frac{f}{r-f}(rN^L - N^T). \quad (11)$$

In the dilepton analysis, fake leptons can originate from QCD multijet events and  $W(\rightarrow l\nu_l) + \text{jets}$ . Due to the presence of two leptons in the event, one of the leptons is required to be tight, while the other lepton is required to pass the loose selection criteria in the loose sample (which corresponds to a number of events  $N^{TL}$ ), or the tight selection criteria in the tight sample (which corresponds to a number of events  $N^{TT}$ ). In turn, using the same formalism as in the single-lepton channel, the total fake-lepton contribution in the dilepton events,  $N_f^{TT}$ , can be written as:

$$N_f^{TT} = \frac{f}{r-f}(rN^{TL} - N^{TT}). \quad (12)$$

The main ingredients of the data-driven method used to estimate the contribution of fake leptons are the efficiencies  $r$  and  $f$  for a true lepton to be identified as a real lepton and for a fake lepton to be mis-identified as a real lepton, respectively. The measurement of the lepton identification efficiency  $r$  is derived using a tag-and-probe method in data  $Z \rightarrow l^+l^-$  events with a dilepton invariant mass in the range

86–96 GeV, where one lepton is required to fulfil tight selection criteria. The rate at which the other lepton passes the same tight selection criteria defines  $r$ . On the other hand, a control sample with fake leptons is selected by considering data events with exactly one lepton passing the loose criteria. To select events dominated by QCD processes,  $E_T^{\text{miss}}$  is required to be between 5 and 20 GeV. After subtraction of other SM processes with true leptons, the rate at which a loose lepton passes tight selection criteria defines the fake rate  $f$ . In the final parameterisation of the efficiencies  $r$  and  $f$ , any significant dependence on kinematical or topological observables such as the transverse momentum and pseudorapidity of the lepton, the jet multiplicity, the number of  $b$ -tagged jets, etc, are taken into account.

## 5 Study of Single-Lepton Events

### 5.1 Event selection

In order to select single-lepton  $t\bar{t}$  events for the charged Higgs boson search, the following cuts are applied to the data and Monte Carlo samples:

- exactly one trigger-matched lepton with  $E_T > 25$  GeV (electron) or  $p_T > 20$  GeV (muon),
- at least four jets with  $p_T > 20$  GeV and  $|\eta| < 2.5$ , including exactly two  $b$ -tagged jets,
- to select events with a large  $E_T^{\text{miss}}$  while rejecting those in which the latter mostly arises from badly reconstructed leptons (i.e. where the azimuthal angle  $\phi_{l,\text{miss}}$  between the lepton and  $E_T^{\text{miss}}$  is small), we demand that:

$$\begin{aligned} E_T^{\text{miss}} &> 40 \text{ GeV} & \text{if } |\phi_{l,\text{miss}}| \geq \pi/6, \\ E_T^{\text{miss}} \times |\sin(\phi_{l,\text{miss}})| &> 20 \text{ GeV} & \text{if } |\phi_{l,\text{miss}}| < \pi/6. \end{aligned}$$

Having selected single-lepton  $t\bar{t}$  events, the jets must be assigned correctly, and in particular the  $b$ -jet that belongs to the leptonic side of the event must be identified. For this purpose, we iterate over all selected jets and find the combination of one  $b$ -jet and two light-quark jets ( $j$ ) that minimises:

$$\chi^2 = \frac{(m_{jjb} - m_{\text{top}})^2}{\sigma_{\text{top}}^2} + \frac{(m_{jj} - m_W)^2}{\sigma_W^2}, \quad (13)$$

where  $\sigma_{\text{top}}$  and  $\sigma_W$  are the assumed widths of the reconstructed top-quark and  $W$  boson, as estimated from correctly-identified combinations in simulated  $t\bar{t}$  events. The corresponding assignment efficiency is 74%. At this stage, events are removed if  $\chi^2 > 5$ . Events having a second lepton with  $E_T > 15$  GeV (electron) or  $p_T > 15$  GeV (muon) are also discarded.

In the presence of a charged Higgs boson, one can not rely on the predicted cross-section of 165 pb<sup>-1</sup> for  $t\bar{t}$  decaying into the  $bbWW$  final state. Therefore, a control region enriched with SM-like  $t\bar{t}$  events is defined, based on the variable  $\cos\theta_l^*$  (see Section 5.2), where a fiducial cross section  $\sigma_{bbWW}$  can be measured for the  $t\bar{t} \rightarrow b\bar{b}W^+W^-$  process. Because  $t\bar{t} \rightarrow b\bar{b}H^\pm W^\mp$  and  $t\bar{t} \rightarrow b\bar{b}H^+H^-$  events may also be found in the control region,  $\sigma_{bbWW}$  is treated as a free parameter when the upper limits on the branching fraction  $\mathcal{B}(t \rightarrow bH^+)$  are derived, see Section 7. With  $B \equiv \mathcal{B}(t \rightarrow bH^+)$ , the cross sections  $\sigma_{bbHW}$  and  $\sigma_{bbHH}$  for  $t\bar{t} \rightarrow b\bar{b}H^\pm W^\mp$  and  $t\bar{t} \rightarrow b\bar{b}H^+H^-$ , respectively, are then given by:

$$\sigma_{bbHW} = \sigma_{bbWW} \times \frac{2B}{1-B}, \quad (14)$$

$$\sigma_{bbHH} = \sigma_{bbWW} \times \frac{B^2}{(1-B)^2}. \quad (15)$$

Table 2 shows how the event selection affects the SM processes and  $t\bar{t}$  events with at least one decay  $t \rightarrow bH^+$ , assuming  $m_{H^+} = 130$  GeV and a cross section of 38.7 pb. A value of 165.1 pb is used for  $\sigma_{bbWW}$ , as obtained when setting the exclusion limit for that mass point, and  $\mathcal{B}(t \rightarrow bH^+) = 10\%$ . Events surviving the selection cuts are dominantly single-lepton  $t\bar{t}$  events, as expected.

$t\bar{t}$ ( $bbWW$ )	Single top-quark	W+jets	Z+jets	Diboson	QCD	$\sum$ SM	Data	130 GeV $H^+$ $\mathcal{B}(t \rightarrow bH^+) = 10\%$
3081	88	85	5.2	2.0	56	3317	3421	190

Table 2: Number of selected events for the simulated processes in the single-lepton channel (here, a fitted value of 165.1 pb is used for  $\sigma_{bbWW}$ ) and comparison with  $1.03 \text{ fb}^{-1}$  of ATLAS data.

## 5.2 Reconstruction of the discriminating variables

On the leptonic side of the event, by using the charged lepton and the associated  $b$ -jet, the variable  $\cos \theta_l^*$  can be computed. The left-hand plot of Fig. 1 shows the  $\cos \theta_l^*$  distribution obtained in ATLAS data and Monte Carlo simulations. The control region enriched with  $t\bar{t} \rightarrow b\bar{b}W^+W^-$  events is defined by requiring  $-0.2 < \cos \theta_l^* < 1$ . In contrast, in order to select a signal region enriched with  $t\bar{t} \rightarrow b\bar{b}H^\pm W^\mp$  and  $t\bar{t} \rightarrow b\bar{b}H^+H^-$  events,  $\cos \theta_l^* < -0.6$  is required, as indicated by the arrow. Also, in order to enhance decays of charged ( $W$  or Higgs) bosons via  $\tau \rightarrow l\nu/\nu\tau$ , we demand that  $m_T^W < 60$  GeV. For the events found in this signal region, the transverse mass  $m_T^H$  is used as a discriminating variable to search for charged Higgs bosons, as illustrated by the right-hand plot of Fig. 1. The ATLAS data is found to agree well with the SM expectations and neither an excess of events (with respect to the prediction for  $t\bar{t} \rightarrow b\bar{b}W^+W^-$  events) nor a significant deformation of the  $m_T^H$  distribution is observed.

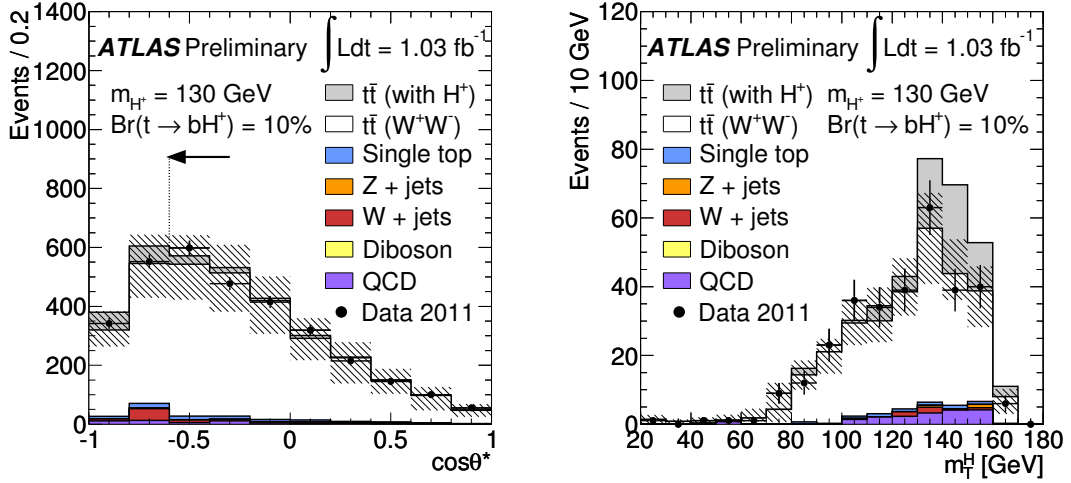


Figure 1: Reconstruction of  $\cos \theta_l^*$  (left) on the leptonic side of the single-lepton events and of the transverse mass  $m_T^H$  (right) when  $\cos \theta_l^* < -0.6$  and  $m_T^W < 60$  GeV, in ATLAS data and Monte Carlo simulations. A fitted value of 165.1 pb is used for  $\sigma_{bbWW}$  and the striped area shows the systematic uncertainties for the SM backgrounds (see Section 7.2). The grey histogram shows the predicted contribution of events with a 130 GeV charged Higgs boson, assuming  $\mathcal{B}(t \rightarrow bH^+) = 10\%$  and  $\mathcal{B}(H^+ \rightarrow \tau\nu) = 1$ .

## 6 Study of Dilepton Events

### 6.1 Event selection

In order to select dilepton  $t\bar{t}$  events for charged Higgs boson searches, the following cuts are applied:

- exactly two oppositely charged leptons, including at least one matched to the single-lepton trigger with  $E_T > 25$  GeV (electron) or  $p_T > 20$  GeV (muon),
- at least two jets with  $p_T > 20$  GeV and  $|\eta| < 2.5$ , including exactly two  $b$ -tagged jets,
- for  $ee$  and  $\mu\mu$  events, the dilepton invariant mass  $m_{ll}$  must be larger than 15 GeV and must satisfy  $|m_{ll} - m_Z| > 10$  GeV (i.e.  $Z$  veto), together with  $E_T^{\text{miss}} > 40$  GeV,
- for  $e\mu$  events, the scalar sum of the transverse energies of the two leptons and all selected jets must satisfy  $\sum E_T > 130$  GeV.

There is a four-fold ambiguity in assigning the two leptons and the two  $b$ -jets to their parents. In the first stage, we try to determine the correct  $l$ - $b$  pairing by selecting only those events which have an easy-to-find incorrect pairing. These are identified as having  $\cos \theta_l^* > 1$  for either of the two  $l$ - $b$  pairs. For such events with a clear incorrect pairing, the other  $l$ - $b$  combinations are chosen, provided that they have  $\cos \theta_l^* < 1$ . For the events with  $\cos \theta_l^* < 1$  for all pairings, the two  $l$ - $b$  pairs that minimise the sum of the distances  $\Delta R(l, b)_{\text{pair 1}} + \Delta R(l, b)_{\text{pair 2}}$  in the  $\eta$ - $\phi$  plane are chosen. In simulated  $t\bar{t}$  events, the assignment efficiency is 66%. The particles of the  $l$ - $b$  pair with the smallest  $\cos \theta_l^*$  value are then assigned to the “ $H^+$  side” and its partner pair to the “ $W$  side”. In simulated events with a 130 GeV charged Higgs boson, this second assignment has an efficiency of 62%. The events for which the numerical computation of  $m_{T2}^H$  does not converge are discarded.

Again, since one can not rely on the predicted value of 165 pb for the cross section of  $t\bar{t} \rightarrow b\bar{b}W^+W^-$  production, a control region enriched with such SM-like events is defined, based on the variable  $\cos \theta_l^*$  (see Section 6.2), in order to measure a fiducial cross section for  $t\bar{t} \rightarrow b\bar{b}W^+W^-$  when the upper limits on  $\mathcal{B}(t \rightarrow bH^+)$  are derived, see Section 7. In the dilepton channel, a downward fluctuation of data in the control region yields fitted values of  $\sigma_{bbWW}$  slightly smaller than the SM prediction. Table 3 shows that events surviving the selection cuts detailed above are dominantly dilepton  $t\bar{t}$  events. The expected number of events for a Monte Carlo  $t\bar{t}$  sample with at least one decay  $t \rightarrow bH^+$  is also shown in the last column, assuming  $m_{H^+} = 130$  GeV and a cross section of 35.3 pb. It corresponds to a fitted value of 150.4 pb for  $\sigma_{bbWW}$  (as obtained when setting the exclusion limit for that mass point) and  $\mathcal{B}(t \rightarrow bH^+) = 10\%$ .

$t\bar{t}$ ( $bbWW$ )	Single top-quark	$Z$ +jets	Diboson	QCD and $W$ +jets	$\sum$ SM	Data	130 GeV $H^+$ $\mathcal{B}(t \rightarrow bH^+) = 10\%$
864	18	1.5	0.3	40	924	992	115

Table 3: Number of selected events for the simulated processes in the dilepton analysis (here, a fitted value of 150.4 pb is used for  $\sigma_{bbWW}$ ) and comparison with  $1.03 \text{ fb}^{-1}$  of ATLAS data.

### 6.2 Reconstruction of the discriminating variables

The left-hand plot of Fig. 2 shows the  $\cos \theta_l^*$  distribution on the “ $H^+$  side” in ATLAS data and Monte Carlo simulations. Here, the control region enriched with  $t\bar{t} \rightarrow b\bar{b}W^+W^-$  events is defined by requiring  $-0.4 < \cos \theta_l^* < 1$  and, in order to select a signal region enriched with  $t\bar{t} \rightarrow b\bar{b}H^\pm W^\mp$  and  $t\bar{t} \rightarrow b\bar{b}H^+H^-$

events,  $\cos \theta_l^* < -0.6$  is required on the “ $H^+$  side”, as indicated by the arrow. For the events found in this signal region, the generalised transverse mass  $m_{T2}^H$  is used as a discriminating variable to search for charged Higgs bosons, as illustrated by the right-hand plot of Fig. 2. Neither an excess of events (with respect to the prediction for  $t\bar{t} \rightarrow b\bar{b}W^+W^-$  events) nor a significant deformation of the  $m_{T2}^H$  distribution is observed.

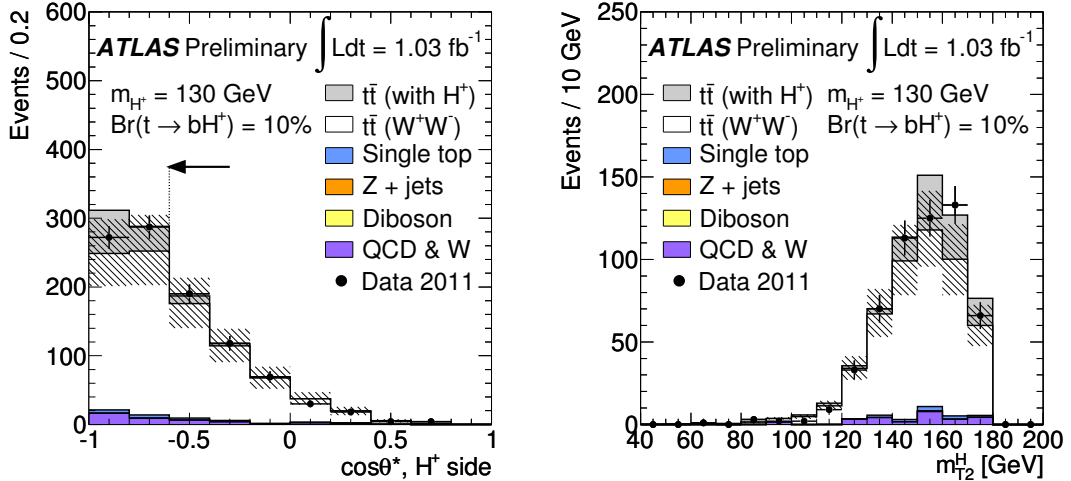


Figure 2: Reconstruction of  $\cos \theta_l^*$  on the “ $H^+$  side” of the dilepton events (left) and of the generalised transverse mass  $m_{T2}^H$  (right) when  $\cos \theta_l^* < -0.6$ , in ATLAS data and Monte Carlo simulations. A fitted value of 150.4 pb is used for  $\sigma_{bbWW}$  and the striped area shows the systematic uncertainties for the SM backgrounds (see Section 7.2). The grey histogram shows the predicted contribution of events with a 130 GeV charged Higgs boson, assuming  $\mathcal{B}(t \rightarrow bH^+) = 10\%$  and  $\mathcal{B}(H^+ \rightarrow \tau\nu) = 1$ .

## 7 Limits on the Branching Ratio of $t \rightarrow bH^+$

### 7.1 Method

Assuming  $\mathcal{B}(H^+ \rightarrow \tau\nu) = 1$ , upper limits are extracted on the branching ratio  $B \equiv \mathcal{B}(t \rightarrow bH^+)$  as a function of the charged Higgs boson mass. Since the signal and the  $t\bar{t}$  background are correlated, the event rate of the  $t\bar{t} \rightarrow b\bar{b}W^+W^-$  background is derived from the measurement in the control region (CR) with  $-0.2 < \cos \theta_l^* < 1$  in the single-lepton analysis or  $-0.4 < \cos \theta_l^* < 1$  in the dilepton analysis, while the signal region (SR) corresponds to  $\cos \theta_l^* < -0.6$  (with the additional cut  $m_T^W < 60$  GeV in the single-lepton case). Let  $\mu_W$  be the expected number of SM-like  $t\bar{t} \rightarrow b\bar{b}W^+W^-$  background events and let  $\mu_{\text{others}}$  be the expected background from other SM processes. For any branching fraction  $B$ , the expected number of  $t\bar{t} \rightarrow b\bar{b}H^\pm W^\mp$  events,  $\mu_H$ , is given by:

$$\mu_H = \mu_W \times \frac{2B}{1 - B}. \quad (16)$$

Note that  $t\bar{t} \rightarrow b\bar{b}H^+H^-$  events are not considered in the following. Other searches for charged Higgs bosons, such as the one reported in Ref. [10], indeed suggest that top-quarks decay into  $bH^+$  in less than 10% of the cases, hence the contribution from  $t\bar{t} \rightarrow b\bar{b}H^+H^-$  remains very small. By not considering these events, our estimation of the upper limit on  $\mathcal{B}(t \rightarrow bH^+)$  is somewhat conservative.

We first focus on the control region of the  $\cos \theta_l^*$  distribution. If  $\epsilon_W$  and  $\epsilon_H$  are the corresponding acceptances of the SM-like  $t\bar{t} \rightarrow b\bar{b}W^+W^-$  events and of the signal  $t\bar{t} \rightarrow b\bar{b}H^\pm W^\mp$  events (derived from Monte Carlo simulations), the expected number of events in the control region is:

$$\mu^{\text{CR}} = \mu_W \epsilon_W + \mu_H \epsilon_H + \mu_{\text{others}}^{\text{CR}} = \mu_W \left( \epsilon_W + \frac{2B}{1-B} \epsilon_H \right) + \mu_{\text{others}}^{\text{CR}}. \quad (17)$$

Let now  $\delta_W$  and  $\delta_H$  be scaling factors from the control region to the signal region (also derived from Monte Carlo simulations). The expected number of events in the signal region is:

$$\mu^{\text{SR}} = \mu_W \epsilon_W \delta_W + \mu_H \epsilon_H \delta_H + \mu_{\text{others}}^{\text{SR}} = \mu_W \left( \epsilon_W \delta_W + \frac{2B}{1-B} \epsilon_H \delta_H \right) + \mu_{\text{others}}^{\text{SR}}. \quad (18)$$

Let  $m$  and  $n$  be the number of observed events in the control and signal regions, respectively. In the signal region, the simulated (generalised) transverse mass distributions are described using a probability density function  $f_i(m_T)$ . The expected and observed number of events in each bin  $i$  are thus respectively  $\mu_i^{\text{SR}} = \mu^{\text{SR}} f_i(m_T)$  and  $n_i$ . The resulting likelihood is given by:

$$\mathcal{L}(B) = \text{Poisson}(m|\mu^{\text{CR}}) \prod_i \text{Poisson}(n_i|\mu_i^{\text{SR}}) \prod_j p(\tilde{\theta}_j|\theta_j), \quad (19)$$

where the index  $i$  indicates the bin of the discriminating transverse mass variable distribution. Nuisance parameters  $\theta$  are used to describe the effect of systematic uncertainties, and  $p(\tilde{\theta}_j|\theta_j)$  are the Gaussian constraints relating each parameter to its nominal estimate  $\tilde{\theta}_j$ . We perform a profile likelihood statistical analysis with  $B$  as the one parameter of interest and  $\mu_W$  as an additional nuisance parameter that is only constrained by data in the control and signal regions. The test statistic is given by [41]:

$$q_B = -2 \log \frac{\mathcal{L}(B, \hat{\theta}_B, \hat{\mu}_{W,B})}{\mathcal{L}(\hat{B}, \hat{\theta}, \hat{\mu}_W)}, \quad 0 \leq \hat{B} \leq B, \quad (20)$$

where  $\hat{\theta}_B$  and  $\hat{\mu}_{W,B}$  are the maximum likelihood estimators (MLE) of the nuisance parameters for a fixed  $B$ , while  $\hat{\theta}$ ,  $\hat{\mu}_W$  and  $\hat{B}$  are the global MLEs of  $\theta$ ,  $\mu_W$  and  $B$ , respectively. The limit itself is derived using the CLs criterion [42] based on a fully frequentist ensemble in which  $n_i$ ,  $m$  and  $\tilde{\theta}_j$  are randomised.

## 7.2 Systematic uncertainties

All systematic uncertainties arising from the measurement of the integrated luminosity and the object reconstruction in ATLAS are considered. These are mostly related to trigger, reconstruction and identification (ID) efficiencies, as well as the energy/momentum resolution and scale of the objects described above. To assess the impact of most sources of systematic uncertainty on the result of the analysis, the selection cuts for each analysis are re-applied after shifting a particular parameter by its  $\pm 1$  standard deviation uncertainty.

To estimate the systematic uncertainty arising from the  $t\bar{t}$  generation and the parton shower model, the acceptance is computed for  $t\bar{t}$  events produced with MC@NLO interfaced to HERWIG/JIMMY or POWHEG [43] interfaced to PYTHIA. For the signal samples, which are generated with PYTHIA (i.e. at the leading order only), no alternative generator is available. Instead, the systematic uncertainty for the signal samples is set to the relative difference in acceptance between  $t\bar{t}$  events generated with MC@NLO interfaced to HERWIG/JIMMY or AcerMC [44], which is also a leading-order generator, interfaced to PYTHIA. The systematic uncertainties arising from initial and final state radiation are computed using  $t\bar{t}$

samples generated with AcerMC and PYTHIA, where initial and final state radiation parameters are set to a range of values not excluded by the experimental data. The largest relative differences with respect to the reference sample in the signal region are used as systematic uncertainties.

In the single-lepton channel, the  $W$ +jets background is not precisely predicted, especially after the  $b$ -tagging requirement. Hence, a factor 2 up/down normalisation uncertainty is assigned to the Monte Carlo  $W$ +jets background sample, with an associated log-normal constraint.

In the data-driven methods used to identify events with fake leptons, the main systematic uncertainties arise from the sample dependence (the fake efficiencies are calculated in a control region dominated by gluon-initiated events, but are later used in a data sample with a higher fraction of quark-initiated events) and from the Monte Carlo samples used for the subtraction of real leptons in the determination of the fake efficiencies, which are sensitive to the dominant instrumental systematic uncertainties.

A summary of the systematic uncertainties considered in this study and their treatment in the analysis are given in Table 4.

Source of uncertainty	Treatment in analysis
Integrated luminosity	$\pm 3.7\%$ [32].
Electron trigger efficiency	$\pm (0.4\text{--}1.0)\%$ , depending on $\eta$ .
Electron reco. efficiency	$\pm (0.7\text{--}1.8)\%$ , depending on $\eta$ .
Electron ID efficiency	$\pm (2.2\text{--}3.8)\%$ , depending on $E_T$ and $\eta$ .
Electron energy scale	$\pm (0.3\text{--}1.8)\%$ , additional constant term, depending on $p_T$ and $\eta$ .
Electron energy resolution	$\pm (0.5\text{--}2.4)\%$ , depending on $p_T$ and $\eta$ .
Muon trigger efficiency	$\pm (0.5\text{--}7.9)\%$ , depending on $p_T$ , $\eta$ , $\phi$ and the data-taking period.
Muon reco. efficiency	$\pm (0.4\text{--}0.8)\%$ , depending on $E$ , $\eta$ , $\phi$ .
Muon ID efficiency	Scale factor = $1.0008 \pm 0.0004$ .
Muon momentum scale and resolution	Up to $\pm 1\%$ , depending on $p_T$ and $\eta$ .
Jet energy resolution (JER)	$\pm (10\text{--}30)\%$ , depending on $p_T$ and $\eta$ .
Jet energy scale (JES)	$\pm (2.5\text{--}14)\%$ , depending on $p_T$ and $\eta$ , + pile-up term (2–7%) in quadrature.
Jet reconstruction efficiency	Randomly drop jets (2%) from the events and symmetrise.
$b$ -tagging efficiency	$\pm (5.7\text{--}15.5)\%$ , depending on $p_T$ .
$b$ -tagging mistag rate	$\pm (10\text{--}21)\%$ , depending on $p_T$ and $\eta$ .
$b$ -jet JES uncertainty	$\pm (1.1\text{--}3.2)\%$ , depending on $p_T$ , added to the standard JES.
$E_T^{\text{miss}}$ uncertainty	Uncertainties from object scale and resolution + 10% flat pile-up contribution.
Event generation and parton shower	Single-lepton analysis: 5.1% for $t\bar{t}$ , 9.1% for the signal (in SR). Dilepton analysis: 6.2% for $t\bar{t}$ , 3.9% for the signal (in SR).
Initial and final state radiation	Single-lepton analysis: 7.9%. Dilepton analysis: 7.7%.
$W$ +jets (single-lepton channel)	Factor 2 up/down with an associated log-normal constraint.
Data-driven methods used to identify events with fake leptons	Single-lepton analysis: 32%. Dilepton analysis: 28%.

Table 4: Main systematic uncertainties considered in this analysis.

### 7.3 Results

Figure 3 shows the 95% confidence level (C.L.) upper limits on the branching fraction  $\mathcal{B}(t \rightarrow bH^+)$ , obtained with the assumption that  $\mathcal{B}(H^+ \rightarrow \tau\nu) = 1$ . In the single-lepton channel, the fitted values of  $\mu_W$  lie between 0.99 and 1.03 times the SM prediction, with uncertainties in the range 2–3%. In the dilepton channel, a downward fluctuation of data in the control region yields fitted values of  $\mu_W$  between 0.78 and 1.06 times the SM prediction, with uncertainties in the range 5–25%. When a charged Higgs boson mass of 160 GeV is assumed, the  $b$ -jets coming from  $t \rightarrow bH^+$  are usually so soft that they are not likely to survive the  $p_T$  cut at 20 GeV, leading to a significant loss of sensitivity for that mass point.

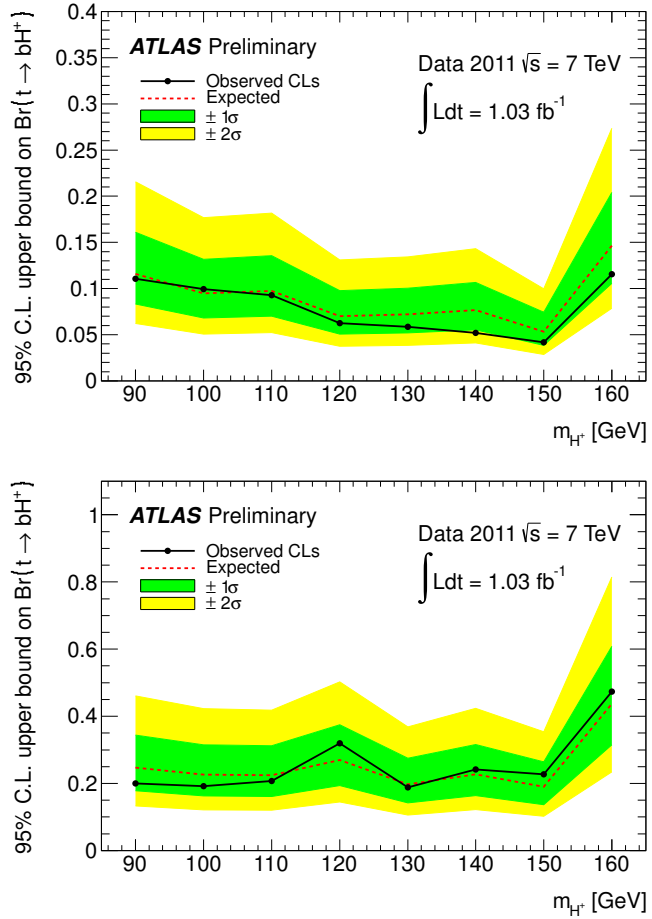


Figure 3: Upper limits on  $\mathcal{B}(t \rightarrow bH^+)$  in the single-lepton (top) and dilepton (bottom) channels, as a function of the charged Higgs boson mass, obtained for an integrated luminosity of  $1.03 \text{ fb}^{-1}$  and with the assumption that  $\mathcal{B}(H^+ \rightarrow \tau\nu) = 1$ . All systematic uncertainties are included, as described in the text. Solid lines denote the observed 95% C.L. upper limits, while dashed lines represent the expected limits. The outer edges of the green and yellow shaded regions show the  $1\sigma$  and  $2\sigma$  error bands.

Since the two channels considered in this study are orthogonal, a combined exclusion limit can be computed. For this purpose, the systematic uncertainties are assumed to be 100% correlated. Although the expected limit improves after the combination, the observed combined limit on  $\mathcal{B}(t \rightarrow bH^+)$  is actually found to be slightly worse when combining the two analyses than for the single-lepton channel only, see Fig. 4 and Table 5. The compatibility with background is measured by  $p_0$ -values, which range between 26% and 50%. Hence, no indication of an  $H^+$ -like excess is found.

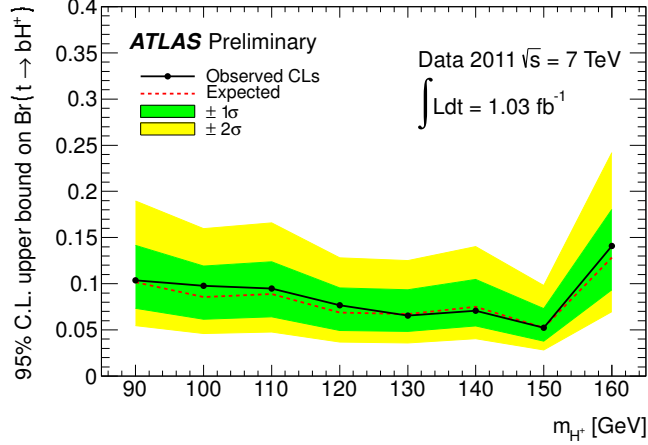


Figure 4: Upper limits on  $\mathcal{B}(t \rightarrow bH^+)$  for the combined single-lepton and dilepton channels, as a function of the charged Higgs boson mass, obtained for an integrated luminosity of  $1.03 \text{ fb}^{-1}$  and with the assumption that  $\mathcal{B}(H^+ \rightarrow \tau\nu) = 1$ .

$m_{H^+}$ (GeV)	90	100	110	120	130	140	150	160
95% C.L. observed (expected) limit on $\mathcal{B}(t \rightarrow bH^+)$ for the single-lepton channel	11.1% (11.6%)	9.9% (9.5%)	9.3% (9.7%)	6.3% (7.0%)	5.8% (7.2%)	5.2% (7.7%)	4.2% (5.3%)	11.6% (14.6%)
95% C.L. observed (expected) limit on $\mathcal{B}(t \rightarrow bH^+)$ for the dilepton channel	20.0% (24.7%)	19.2% (22.6%)	20.7% (22.4%)	32.0% (26.9%)	18.8% (19.8%)	24.2% (22.6%)	22.7% (19.0%)	47.3% (43.7%)
95% C.L. observed (expected) limit on $\mathcal{B}(t \rightarrow bH^+)$ for the combined channels	10.4% (10.2%)	9.8% (8.5%)	9.5% (8.9%)	7.7% (6.9%)	6.6% (6.7%)	7.1% (7.5%)	5.2% (5.2%)	14.1% (12.9%)

Table 5: Observed (expected) 95% C.L. upper limits on  $\mathcal{B}(t \rightarrow bH^+)$  in the single-lepton and dilepton channels, and after their combination, as a function of the charged Higgs boson mass, obtained for an integrated luminosity of  $1.03 \text{ fb}^{-1}$  and with the assumption that  $\mathcal{B}(H^+ \rightarrow \tau\nu) = 1$ .

Finally, Fig. 5 shows the upper limit in the context of the  $m_h^{\max}$  scenario of the MSSM [45], in the  $m_{H^+}$ - $\tan\beta$  plane. No exclusion limit is shown for charged Higgs boson masses above 140 GeV since no reliable calculations of  $\mathcal{B}(t \rightarrow bH^+)$  exist for  $\tan\beta$  values in the range of interest. Also, since the assumption  $\mathcal{B}(H^+ \rightarrow \tau\nu) = 1$  is not fulfilled at low  $\tan\beta$ , we do not attempt to derive limits in this region. The following relative uncertainties on  $\mathcal{B}(t \rightarrow bH^+)$  are considered and added linearly [46]:

- 5% for one-loop electroweak corrections missing in the calculations,
- 2% for missing two-loop QCD corrections,
- about 1% (depending on  $\tan\beta$ ) for  $\Delta_b$ -induced uncertainties, where  $\Delta_b$  is a correction factor to the running  $b$ -quark mass [47].

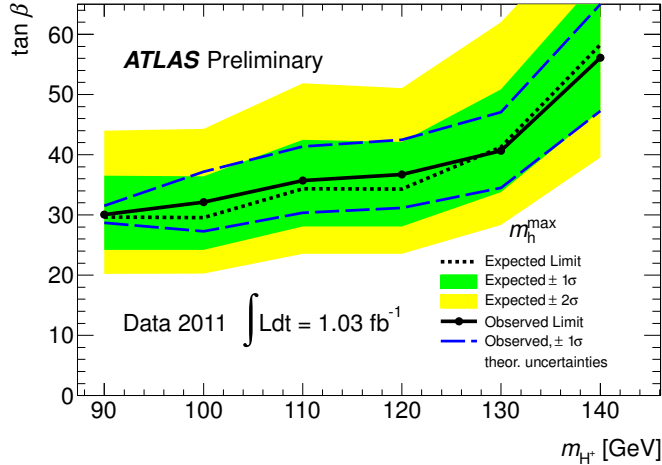


Figure 5: Limits for charged Higgs boson production from top-quark decays in the  $m_{H^+}$ - $\tan\beta$  plane, in the context of the  $m_h^{\max}$  scenario of the MSSM, obtained for an integrated luminosity of  $1.03 \text{ fb}^{-1}$  and with the assumption that  $\mathcal{B}(H^+ \rightarrow \tau\nu) = 1$ . The  $1\sigma$  band around the observed limit (blue dashed lines) is obtained by adjusting the theoretical uncertainties listed in the text and adding them linearly.

## 8 Conclusion

This paper presents the results of a search for charged Higgs bosons by the ATLAS experiment, based on  $1.03 \text{ fb}^{-1}$  of proton-proton collision data at  $\sqrt{s} = 7 \text{ TeV}$  using the single-lepton and dilepton channels in  $t\bar{t}$  decays with a leptonically decaying  $\tau$  in the final state. New discriminating variables were identified in order to distinguish between leptons produced in  $\tau$  decays and leptons arising directly from  $W$  boson decays. In both (single-lepton and dilepton) channels, the data agree well with the SM expectation. Hence, assuming  $\mathcal{B}(H^+ \rightarrow \tau\nu) = 1$ , this leads to upper limits on the branching fraction  $\mathcal{B}(t \rightarrow bH^+)$  between 5.2% and 14.1% for charged Higgs boson masses in the range  $90 \text{ GeV} < m_{H^+} < 160 \text{ GeV}$ . This result constitutes an improvement compared to the limits provided by the Tevatron experiments. Except for the mass point at 160 GeV, our exclusion limits are also comparable to (or somewhat higher than) those presented by CMS in Ref. [9] and by ATLAS in Ref. [10]. In the context of the  $m_h^{\max}$  scenario of the MSSM, values of  $\tan\beta$  larger than 30–56 are excluded in the mass range  $90 \text{ GeV} < m_{H^+} < 140 \text{ GeV}$ .

## References

- [1] J. F. Gunion, H. E. Haber, G. Kane, and S. Dawson, *The Higgs Hunter's Guide*. Addison-Wesley, 1990.
- [2] J. F. Gunion, H. E. Haber, G. L. Kane, and S. Dawson, *Errata for "The Higgs Hunter's Guide"*, [hep-ph/9302272](https://arxiv.org/abs/hep-ph/9302272).
- [3] J. F. Gunion and H. E. Haber, *Higgs Bosons in Supersymmetric Models. 1.*, Nucl. Phys. B **272** (1986) 1.
- [4] K. Inoue, A. Kakuto, H. Komatsu, and S. Takeshita, *Aspects of Grand Unified Models with Softly Broken Supersymmetry*, Prog. Theor. Phys. **68** (1982) 927.
- [5] LHC Higgs Cross Section Working Group Collaboration, S. Dittmaier et al., *Handbook of LHC Higgs Cross Sections: 1. Inclusive Observables*, [arXiv:hep-ph/1101.0593](https://arxiv.org/abs/hep-ph/1101.0593).
- [6] LEP Higgs Working Group for Higgs boson searches Collaboration, *Search for charged Higgs bosons: Preliminary combined results using LEP data collected at energies up to 209 GeV*, [arXiv:hep-ex/0107031](https://arxiv.org/abs/hep-ex/0107031).
- [7] CDF Collaboration, *Search for charged Higgs bosons in decays of top quarks in p-pbar collisions at  $\sqrt{s} = 1.96$  TeV*, Phys. Rev. Lett. **103** (2009) 101803.
- [8] D0 Collaboration, *Search for charged Higgs bosons in top quark decays*, Phys. Lett. B **682** (2009) 278.
- [9] CMS Collaboration,  $H^+ \rightarrow \tau$  in Top quark decays, CMS-PAS-HIG-11-008.
- [10] ATLAS Collaboration, *Search for Charged Higgs Bosons in the  $\tau+jets$  Final State in  $t\bar{t}$  Decays with  $1.03\text{ fb}^{-1}$  of pp Collision Data Recorded at  $\sqrt{s} = 7$  TeV with the ATLAS Experiment*, ATLAS-CONF-2011-138.
- [11] ATLAS Collaboration, *A Search for a light charged Higgs boson decaying to  $cs^-$  in pp collisions at  $\sqrt{s} = 7$  TeV with the ATLAS detector*, ATLAS-CONF-2011-094.
- [12] ATLAS Collaboration, *The ATLAS Experiment at the CERN Large Hadron Collider*, JINST **3** (2008) S08003.
- [13] ATLAS Collaboration, *Measurement of the W boson polarisation in top quark decays in  $0.70\text{ fb}^{-1}$  of pp collisions at  $\sqrt{s} = 7$  TeV with the ATLAS detector*, ATLAS-CONF-2011-122.
- [14] E. Gross and O. Vitells, *Transverse mass observables for charged Higgs boson searches at hadron colliders*, Phys. Rev. D **81** (2010) 055010.
- [15] ATLAS Collaboration, *Study of discriminating variables for charged Higgs boson searches in  $t\bar{t}$  events with leptons, using  $35\text{ pb}^{-1}$  of data from the ATLAS detector*, ATLAS-CONF-2011-018.
- [16] S. Frixione and B. R. Webber, *Matching NLO QCD computations and parton shower simulations*, JHEP **0206** (2002) 029, [arXiv:hep-ph/0204244](https://arxiv.org/abs/hep-ph/0204244).
- [17] P.M. Nadolsky, H.L. Lai, Q.H. Cao, J. Huston, J. Pumplin, D. Stump, W.K. Tung and C.P. Yuan, *Implications of CTEQ global analysis for collider observables*, Phys. Rev. D **78** (2008) 013004.

[18] G. Corcella, I. Knowles, G. Marchesini, S. Moretti, K. Odagiri, et al., *HERWIG 6: An Event generator for hadron emission reactions with interfering gluons (including supersymmetric processes)*, JHEP **0101** (2001) 010, arXiv:hep-ph/0011363.

[19] J. Butterworth, J. R. Forshaw, and M. Seymour, *Multiparton interactions in photoproduction at HERA*, Z. Phys. C **72** (1996) 637, arXiv:hep-ph/9601371.

[20] U. Langenfeld, S. Moch, and P. Uwer, *New results for  $t\bar{t}$  production at hadron colliders*, arXiv:hep-ph/0907.2527.

[21] ATLAS Collaboration, *Measurement of the top-quark pair production cross section with ATLAS in  $pp$  collisions at  $\sqrt{s} = 7$  TeV*, arXiv:hep-ex/1012.1792.

[22] S. Frixione, E. Laenen, P. Motylinski, and B. R. Webber, *Single-top production in MC@NLO*, JHEP **0603** (2006) 092, arXiv:hep-ph/0512250.

[23] M. L. Mangano, M. Moretti, F. Piccinini, R. Pittau, and A. D. Polosa, *ALPGEN, a generator for hard multiparton processes in hadronic collisions*, JHEP **0307** (2003) 001, arXiv:hep-ph/0206293.

[24] J. Pumplin, D.R. Stump, J. Huston, H.L. Lai, P. Nadolsky and W.K. Tung, *New Generation of Parton Distributions with Uncertainties from Global QCD Analysis*, JHEP **07** (2002) 012.

[25] T. Sjöstrand, S. Mrenna, and P. Z. Skands, *PYTHIA 6.4 Physics and Manual*, JHEP **0605** (2006) 026, arXiv:hep-ph/0603175.

[26] Z. Was and P. Golonka, *TAUOLA as tau Monte Carlo for future applications*, Nucl. Phys. Proc. Suppl. **144** (2005) 88.

[27] E. Barberio, B. van Eijk, and Z. Was, *PHOTOS: A Universal Monte Carlo for QED radiative corrections in decays*, Comput. Phys. Commun. **66** (1991) 115.

[28] ATLAS Collaboration, *Charged particle multiplicities in  $pp$  interactions at  $\sqrt{s} = 0.9$  and 7 TeV in a diffractive limited phase-space measured with the ATLAS detector at the LHC and new PYTHIA6 tune*, ATLAS-CONF-2010-031.

[29] ATLAS Collaboration, *First tuning of HERWIG/JIMMY to ATLAS data*, ATL-PHYS-PUB-2010-014.

[30] GEANT4 Collaboration, S. Agostinelli et al., *GEANT4: A simulation toolkit*, Nucl. Instrum. Meth. A **506** (2003) 250.

[31] ATLAS Collaboration, *The ATLAS Simulation Infrastructure*, Eur. Phys. J. C **70** (2010) 823, arXiv:physics.ins-det/1005.4568.

[32] ATLAS Collaboration, *Updated Luminosity Determination in  $pp$  Collisions at  $\sqrt{s} = 7$  TeV using the ATLAS Detector in 2011*, ATLAS-CONF-2011-116.

[33] ATLAS Collaboration, *Electron performance measurements with the ATLAS detector using the 2010 LHC proton-proton collision data*, arXiv:1110.3174v1 [hep-ex].

[34] ATLAS Collaboration, *Muon reconstruction efficiency in reprocessed 2010 LHC p-p collision data recorded with the ATLAS detector*, ATLAS-CONF-2011-063.

- [35] M. Cacciari, G. P. Salam, and G. Soyez, *The Anti- $k(t)$  jet clustering algorithm*, JHEP **0804** (2008) 063, [arXiv:hep-ph/0802.1189](https://arxiv.org/abs/hep-ph/0802.1189).
- [36] M. Cacciari and G. P. Salam, *Dispelling the  $N^{**}3$  myth for the  $k(t)$  jet-finder*, Phys. Lett. B **641** (2006) 57, [arXiv:hep-ph/0512210](https://arxiv.org/abs/hep-ph/0512210).
- [37] W. Lampl et al., *Calorimeter clustering algorithms: Description and performance*, ATL-LARG-PUB-2008-002.
- [38] ATLAS Collaboration, *Jet energy scale and its systematic uncertainty in proton-proton collisions at  $\sqrt{s} = 7$  TeV in ATLAS 2010 data*, ATLAS-CONF-2011-032.
- [39] ATLAS Collaboration, *Commissioning of the ATLAS high-performance b-tagging algorithms in the 7 TeV collision data*, ATLAS-CONF-2011-102.
- [40] ATLAS Collaboration, *Performance of Missing Transverse Momentum Reconstruction in Proton-Proton Collisions at 7 TeV with ATLAS*, [arXiv:1108.5602v1](https://arxiv.org/abs/1108.5602v1) [hep-ex].
- [41] G. Cowan, K. Cranmer, E. Gross and O. Vitells, *Asymptotic formulae for likelihood-based tests of new physics*, Eur. Phys. J. C **71** (2011) 1554.
- [42] A. Read, *Presentation of search results: The  $CL(s)$  technique*, J. Phys. G **28** (2002) 2693.
- [43] S. Frixione, P. Nason, and C. Oleari, *Matching NLO QCD computations with Parton Shower simulations: the POWHEG method*, JHEP **11** (2007) 070, [arXiv:hep-ph/0709.2092](https://arxiv.org/abs/hep-ph/0709.2092).
- [44] B. P. Kersevan and E. Richter-Was, *The Monte Carlo event generator AcerMC version 2.0 with interfaces to PYTHIA 6.2 and HERWIG 6.5*, [arXiv:hep-ph/0405247](https://arxiv.org/abs/hep-ph/0405247).
- [45] M.S. Carena, S. Heinemeyer, C.E.M. Wagner and G. Weiglein, *Suggestions for benchmark scenarios for MSSM Higgs boson searches at hadron colliders*, Eur. Phys. J. C **26** (2003) 601, [arXiv:hep-ph/0202167](https://arxiv.org/abs/hep-ph/0202167).
- [46] LHC Higgs Cross Section Working Group Collaboration, S. Dittmaier et al., *Handbook of LHC Higgs Cross Sections: 2. Differential Distributions*, in preparation.
- [47] M.S. Carena, D. Garcia, U. Nierste and C.E.M. Wagner, *Effective Lagrangian for the  $\bar{t}bH^+$  interaction in the MSSM and charged Higgs phenomenology*, Nucl. Phys. B **577** (2000) 88, [arXiv:hep-ph/9912516](https://arxiv.org/abs/hep-ph/9912516).